

**Domain formation in rectangular magnetic nanoparticle assemblies**Alexander Fabian,<sup>\*</sup> Michael Czerner, and Christian Heiliger*Institute for Theoretical Physics, Justus Liebig University Giessen, Heinrich-Buff-Ring 16, 35392 Giessen, Germany  
and Center for Materials Research (LaMa), Justus Liebig University Giessen, Heinrich-Buff-Ring 16, 35392 Giessen, Germany*

Matthias T. Elm

*Institute of Experimental Physics I, Justus Liebig University Giessen, Heinrich-Buff-Ring 16, 35392 Giessen, Germany;  
Institute of Physical Chemistry, Justus Liebig University Giessen, Heinrich-Buff-Ring 17, 35392 Giessen, Germany;  
and Center for Materials Research (LaMa), Justus Liebig University Giessen, Heinrich-Buff-Ring 16, 35392 Giessen, Germany*

Detlev M. Hofmann and Peter J. Klar

*Institute of Experimental Physics I, Justus Liebig University Giessen, Heinrich-Buff-Ring 16, 35392 Giessen, Germany  
and Center for Materials Research (LaMa), Justus Liebig University Giessen, Heinrich-Buff-Ring 16, 35392 Giessen, Germany*

(Received 11 May 2018; published 1 August 2018)

Rectangular assemblies with different aspect ratios were prepared with spherical magnetite nanoparticles (diameter  $d = 20$  nm) on lithographically patterned substrates using a variant of the meniscus force deposition method. The aspect ratio (width:length) of the rectangular assemblies was varied from very low (1:1) to very high (1:1000) values. Angle-dependent ferromagnetic resonance measurements were performed to study the influence of the shape anisotropy on the magnetic properties. Using an analytical model based on the Smit-Suhl formalism for single-domain magnets, the demagnetizing factors were determined. The analysis of the resonance signals shows that, for small aspect ratios, the ratio of the in-plane demagnetization factors is inversely proportional to the corresponding ratio of width:length; that is, the assemblies behave like a single ferromagnet due to dipolar magnetic coupling between the particles. At larger aspect ratios a more complicated behavior is observed which indicates the formation of a multidomain-like structure inside the assemblies caused by geometrical inhomogeneities in the filling of the assemblies. Micromagnetic simulations of the magnetic properties of the assemblies support this assumption qualitatively and suggest that the formation of these inhomogeneities can be controlled by the fabrication process. The results provide insights into the collective magnetic behavior of nanoparticle assemblies, highlighting the high degree of tunability of the magnetic properties of such assemblies, which makes them promising building blocks for future magnetic devices.

DOI: [10.1103/PhysRevB.98.054401](https://doi.org/10.1103/PhysRevB.98.054401)**I. INTRODUCTION**

Ferromagnetic nanostructures, such as nanodots, are of high interest in current research since they are more and more utilized for applications in the field of high-density storage media [1–5], nonvolatile logic [6,7], and spintronic devices [8,9]. The large interest arises due to the fact that the magnetic properties of arrays of nanomagnets are determined not only by the magnetic properties of the ferromagnetic material itself, i.e., the chemical composition or its crystal structure, but also by the shape of the nanomagnets which, e.g., is reflected in magnetic phase diagrams of ensembles of such particles [10]. In addition, the interaction between adjacent nanomagnets influences the magnetic properties of such arrangements [11]; for example, the distance between arrays of magnetic nanodisks causes the system's hysteresis to be either soft or hard magnetic [12–14]. Typically, such nanomagnet arrays are prepared by nanostructuring of ferromagnetic thin films, e.g., cobalt or permalloy thin films, using lithographic techniques. The magnetic properties of the arrays are tuned by varying the

size and shape of the individual nanomagnets as well as the distance between them [6,15,16]. An alternative approach is to assemble arrays of magnetic elements using ferromagnetic nanoparticles instead of single atoms as building blocks. As shown by several groups [17–21], low-dimensional assemblies of ferromagnetic nanoparticles show collective magnetic properties due to dipolar coupling between the single particles. As the size of such nanoparticles and their arrangement can be controlled systematically [2,22–25], assemblies of magnetic nanoparticles offer an additional degree of freedom in manipulating the magnetic interactions inside the magnetic elements [26]. Thus, such assemblies are not only promising building blocks for improved magnetic devices but also ideal model systems to study the complex magnetic interactions on different length scales systematically [27]. Magnetite nanoparticles are arranged in micrometer-sized assemblies of rectangular shape which in turn form the magnetic elements of an array. Such samples can be considered to possess three hierarchical levels. Each level corresponds to a different length scale and is tunable individually. One can choose the material and the shape of the nanoparticles on the microscopic level, the size and shape of the magnetic elements on the mesoscopic intermediate level, and, finally, the grid and the shape of the array on

<sup>\*</sup>alexander.fabian@physik.uni-giessen.de

TABLE I. Overview of the parameters of the series of samples with rectangular  $\text{Fe}_3\text{O}_4$  nanoparticle assemblies of different aspect ratios. The parameter  $l_y$  denotes the nearest distance between adjacent assemblies,  $N_i$  are the values deduced for the demagnetizing factors, and  $K_{\text{nu}}$  is the constant describing the influence of the nonuniform demagnetizing field.

Label	Aspect ratio	Real aspect ratio	$N_x$	$N_y$	$N_z$	$N_y/N_x$	$l_y$ ( $\mu\text{m}$ )	$K_{\text{nu}}$ (kerg/cm <sup>3</sup> )
Rect_1	1:1	0.97	2.10	2.10	8.38	1.00	2.00	-1.00
Rect_2	1:2	1.70	0.74	1.11	10.72	1.50	1.70	0.00
Rect_5	1:5	4.00	0.43	1.00	11.14	2.33	2.00	1.50
Rect_10	1:10	7.40	1.60	1.87	9.10	1.17	2.00	6.50
Rect_50	1:50	36.00	0.88	2.14	9.54	2.43	10.00	1.00
Rect_100	1:100	70.00	0.84	2.32	9.41	2.76	11.00	2.00
Rect_200	1:200	134.00	0.19	2.41	9.97	12.68	22.00	3.00
Rect_500	1:500	316.00	0.47	2.22	9.87	4.72	50.00	3.00
Rect_1000	1:1000	815.00	0.54	0.95	11.07	1.76	2.00	2.50

the macroscopic scale. The nanoparticles were assembled using the meniscus force deposition method as described in detail in Refs. [27–29]. Previous studies have shown that on the length scales chosen in this study only the shape of the assemblies has an influence on the magnetic properties [27]. In this work we vary the aspect ratio (width:length) of the assemblies from small to high values, i.e., from 1:1 up to 1:1000, in order to investigate the influence of the assembly's shape on its magnetic properties using angle-dependent ferromagnetic resonance (FMR) measurements. The angle dependence of the resonance field was simulated using a model based on the Smit-Suhl formalism for single-domain magnets yielding the corresponding demagnetization factors. Good agreement with the experimental results was achieved only for aspect ratios below 1:10, revealing the single-magnetic-domain behavior of these assemblies. For longer assemblies the ratios of the demagnetization factors differ distinctly from the expectation given by the aspect ratio of the corresponding assemblies. This behavior is explained by the formation of a multidomainlike structure inside the nanoparticle assemblies due to structural inhomogeneities. This assumption is also supported by micromagnetic simulations.

## II. EXPERIMENTAL METHODS: SAMPLE PREPARATION

Samples with arrays of magnetite nanoparticle assemblies were prepared using a combination of patterned substrates and a horizontal dip-coating process as described in Ref. [27]. In brief, electron-beam lithography was used to transfer the desired pattern of openings onto a resist layer consisting of Poly(methyl methacrylate) (PMMA) on a highly resistive (100) Si substrate. A drop of an aqueous suspension of spherical  $\text{Fe}_3\text{O}_4$  nanoparticles was deposited onto the substrate. The magnetite nanoparticles dispersed in  $\text{H}_2\text{O}$  (particle concentration of about  $4.5 \times 10^{13}$  particles/mL) are commercially available (Sigma-Aldrich, 725366) and have an average diameter of  $(20 \pm 2)$  nm. The substrate was placed horizontally below a cover glass such that the suspension was confined between the two parallel surfaces. By moving the substrate horizontally with respect to the cover glass the nanoparticles were pushed inside the openings of the pattern by the meniscus force occurring at the gap between the edge of the cover glass and the substrate. The assemblies were arranged on rectangular grids, all possessing the same pitch in the  $x$  direction but different

itches in the  $y$  direction depending on the actual length of the assemblies. For both directions, the distance between the assemblies was large enough ( $>1 \mu\text{m}$ ) to exclude an interaction between adjacent assemblies, as shown in previous investigations [27]; that is, it was found that, at such pitches, the FMR signals of arrays of assemblies were affected only by the shape of the assemblies and not by their arrangement in an array on the substrate. The macroscopic array of assemblies and the substrate itself had a square shape for all samples. All arrays had dimensions of  $3 \times 3 \text{ mm}^2$ . A series of nine samples with nanoparticle assemblies with a rectangular shape was prepared, in which the aspect ratio width:height of the assembly was constant for each sample but varied throughout the series from 1:1 up to 1:1000. The width of all assemblies was chosen to be 400 nm, while the length of the assemblies was adjusted according to the aspect ratio from 400 nm up to 400  $\mu\text{m}$ . An overview of the sample parameters is given in Table I. The sample labels correspond to the nominal aspect ratio of the respective rectangular shape. For all aspect ratios compact filling of the openings was achieved, which was confirmed by scanning electron microscopy (SEM). However, inspection of a test sample, which had to be cleaved, suggests that steplike structures arise when filling the elongated openings due to the stepwise movement of the stepper motor. Furthermore, the height of the nanoparticle assemblies decreases from the edges to the center of the opening. Hence, the height of the resulting assemblies varies between 50 and 80 nm, corresponding to two to five monolayers of magnetic spheres. SEM images of three samples with aspect ratios of 1:2, 1:5, and 1:200 and the cleaved sample are shown in Fig. 1.

## III. RESULTS AND DISCUSSION

All samples prepared were investigated by angle-dependent FMR measurements in in-plane and out-of-plane geometry, as schematically shown in Fig. 2. For in-plane geometry, the magnetic field was rotated in the  $x$ - $y$  plane about the  $z$  axis corresponding to a variation of  $\varphi_H \in [0, 2\pi]$  at constant  $\theta_H = \pi/2$  in spherical coordinates. For  $\varphi_H = 0$  ( $\pi/2$ ) the magnetic field was aligned parallel to the longer edge of the rectangular assemblies. To study the out-of-plane geometry the magnetic field was rotated in the  $x$ - $z$  plane about the  $y$  axis corresponding to a variation of  $\theta_H \in [0, 2\pi]$  at constant  $\varphi_H = 0$ . The FMR measurements were conducted at room temperature with a

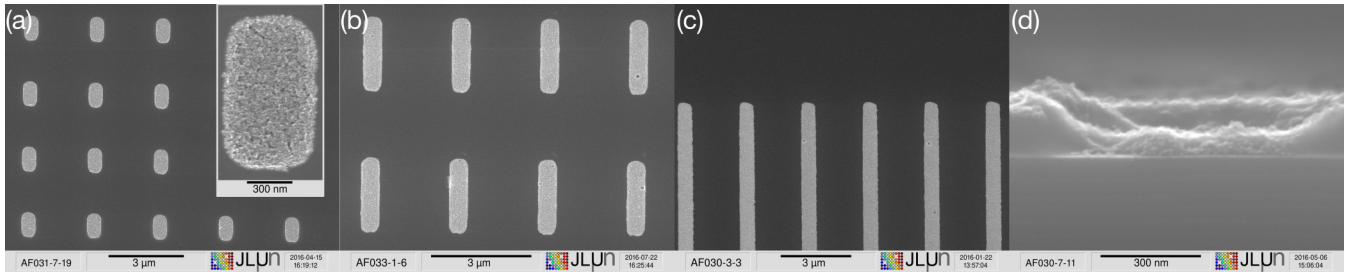


FIG. 1. Examples of  $\text{Fe}_3\text{O}_4$  nanoparticle assemblies prepared on patterned substrates. (a) Aspect ratio of 1:2. The inset shows the magnification of one assembly. (b) Aspect ratio of 1:5. (c) Aspect ratio of 1:200. (d) Side view of a cleaved sample. The filling of the opening shows variations in height.

Bruker ESP 300E spectrometer at  $X$ -band frequencies of about 9.5 GHz. The corresponding spectra are shown in Figs. 2(a) and 2(b) for in-plane and out-of-plane geometry, respectively.

### A. Results for out-of-plane geometry

As shown in Fig. 2, two resonances are required to describe the FMR spectrum when the magnetic field is oriented

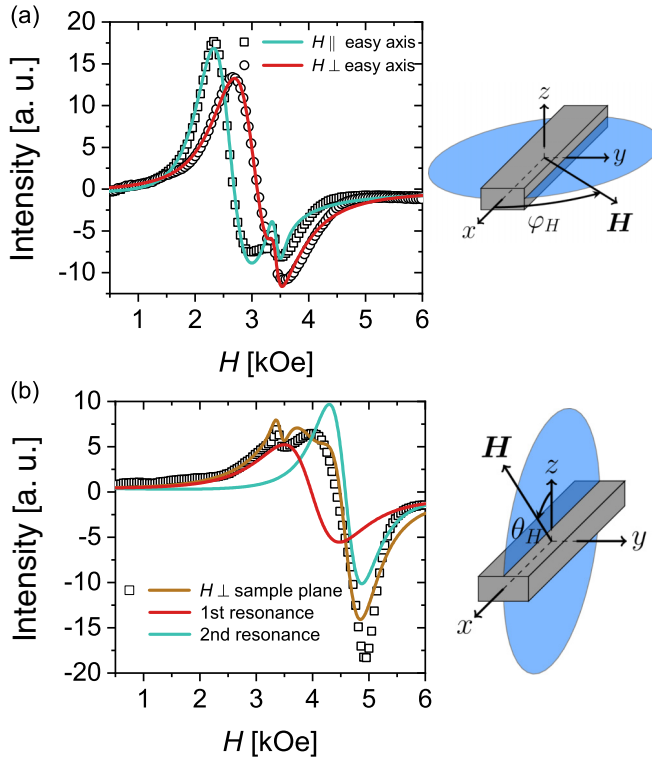


FIG. 2. Measured FMR spectra of Rect\_200 with corresponding fits. (a) In-plane geometry: the spectrum with the lower resonance field corresponds to an orientation of the magnetic field along the easy magnetic axis of the assembly, i.e., the long edge ( $\theta_H = \pi/2$ ,  $\varphi_H = 0$ ). The spectrum with the higher resonance field corresponds to an orientation of the magnetic field along the hard axis, i.e., the short edge ( $\theta_H = \pi/2$ ,  $\varphi_H = \pi/2$ ). Both FMR spectra can be described by one broad resonance. (b) Out-of-plane geometry: the spectrum corresponds to the orientation of the magnetic field perpendicular to the sample plane ( $\theta_H = 0$ ) and exhibits two broad resonances. The fitted curve and the two components describing the two resonances are shown. The sharp feature at about 3.3 kOe is due to impurities in the resonator. It has been accounted for in the fitting process of the spectra.

perpendicular to the sample surface (out-of-plane geometry), while for an in-plane orientation of the magnetic field the two resonances overlap and merge into one broad resonance. The magnetization of a spherical single-magnetic-domain particle should yield only one FMR resonance. However, due to the magnetocrystalline anisotropy the corresponding resonance field may depend on the orientation of the magnetic field with respect to the crystalline axes of the nanoparticle. The occurrence of two resonance signals in the FMR spectra may be related to the random orientation of the spherical nanoparticles in the assemblies [30]. Each sample studied consists of an array of more than a thousand oriented assemblies, where each assembly consists of several hundred single-magnetite nanoparticles. As all the nanoparticles are randomly oriented in the openings, their resonance fields vary according to the different orientations of the underlying cubic crystal structure with respect to the magnetic field direction applied.

Assuming such a situation and noninteracting nanoparticles, the observed FMR spectrum is a sum of the contributions of the individual nanoparticles and is obtained by averaging over the distribution of resonance fields arising from the crystal anisotropy. The corresponding probability density function (PDF)  $\wp(H)$  can be derived following the approach by Winklhofer *et al.* [31]. Because the anisotropy is cubic, it is sufficient to restrict the calculations to 1/16 of the entire orientation space. The calculated resonance fields are shown in Fig. 3(a) as a function of  $\theta$  and  $\varphi$ . The resulting PDF  $\wp(H)$  is shown in Fig. 3(b) and clearly exhibits two maxima. Convoluting  $\wp(H)$  with a Lorentzian resonance line and differentiating the convoluted function with respect to the external magnetic field yields the function presented in Fig. 3(c), which is somewhat similar to the out-of-plane FMR spectrum in Fig. 2(b). The following parameters were used in the calculation. The bulk value  $K_1 = -1.1 \times 10^5 \text{ erg/cm}^3$  for the first anisotropy constant of the cubic magnetocrystalline anisotropy of magnetite [32] and a linewidth of about  $\Delta H = 450 \text{ Oe}$  for the resonance of a single particle. The resemblance of experimental and theoretical FMR spectra justifies describing all the measured FMR spectra using two first derivatives of a Lorentz distribution [33] in order to determine the values of the resonance fields. It should be noted that the discussion above is based on assuming a random distribution of noninteracting spheres exhibiting magnetocrystalline anisotropy. In the case of the rectangular assemblies studied the nanoparticles interact, and the shape anisotropy of the assembly also comes into play. Nevertheless, the discussion motivates the occurrence of two resonances

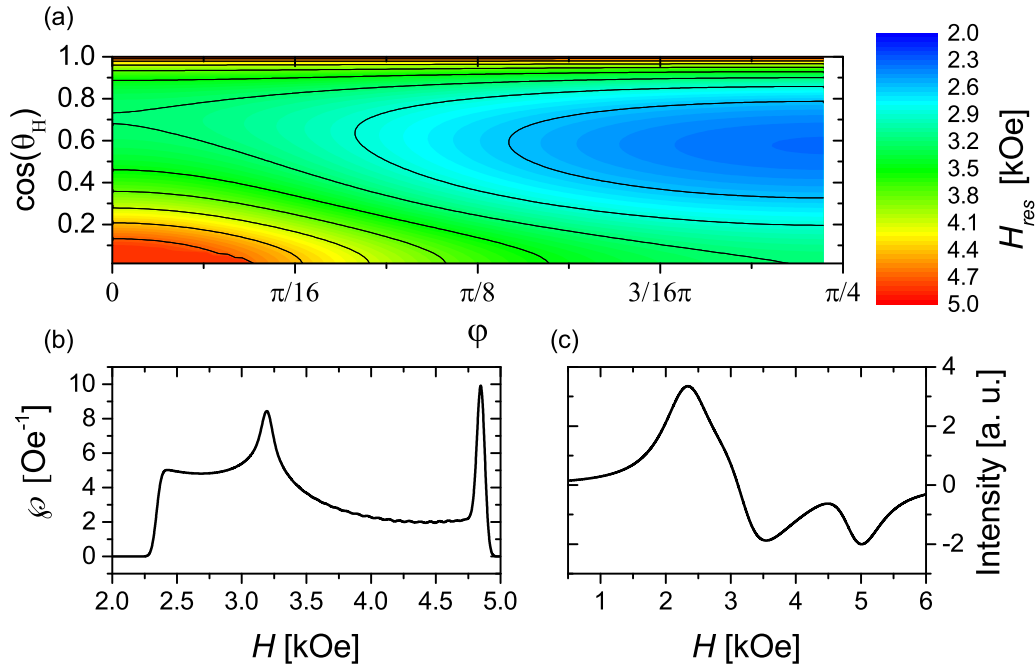


FIG. 3. Results of the powder spectrum calculations for a cubic crystal structure of magnetite. (a) Contour plot of the calculated resonance fields for  $\theta_H \in [0, \pi/2]$  and  $\varphi_H \in [0, \pi/4]$ . (b) Resulting probability density function  $\varphi$  and (c) calculated spectrum of magnetite powder by convolution of the probability density function  $\varphi$  with a Lorentzian line shape function and differentiating with respect to the external magnetic field.

being observed in the FMR spectra for out-of-plane geometry. For all assemblies prepared, the angle dependence of the extracted resonance fields in out-of-plane geometry exhibits a similar trend with a pronounced twofold symmetry and a magnetic easy axis oriented in the sample plane, i.e., visible at  $\theta_H = \pi/2$ . Exemplarily, the angular dependence of the sample Rect\_200 is shown in Fig. 4. Such a twofold angle dependence is expected for an infinitely thin disk of a ferromagnetic single-domain material, which corresponds well to an array of assemblies of interacting nanoparticles on top of a substrate as the height of the assemblies is much smaller than their lateral dimensions. In order to simulate the angle dependence of the

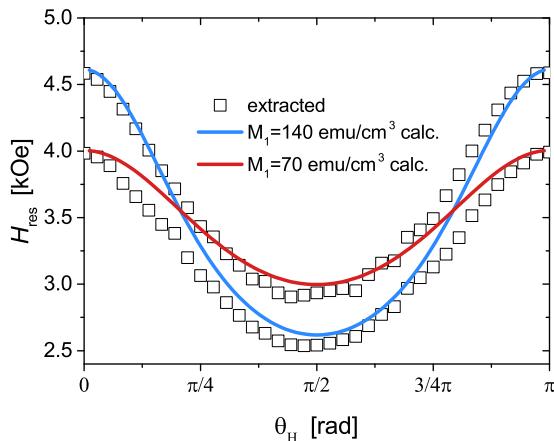


FIG. 4. Angular dependence of the extracted resonance fields in out-of-plane geometry for the sample Rect\_200 with corresponding simulations of both magnetizations,  $M_1 = 140 \text{ emu/cm}^3$  and  $M_2 = 70 \text{ emu/cm}^3$ .

assemblies the Smit-Suhl [34,35] formalism was used,

$$\left(\frac{\omega}{\gamma}\right)^2 = \frac{1}{M^2 \sin^2 \theta} \left[ \frac{\partial^2 U}{\partial \theta^2} \frac{\partial^2 U}{\partial \varphi^2} - \left( \frac{\partial^2 U}{\partial \theta \partial \varphi} \right)^2 \right] \bigg|_{\substack{\theta = \theta_M \\ \varphi = \varphi_M}}, \quad (1)$$

with

$$\frac{\partial U}{\partial \theta} \bigg|_{\theta = \theta_M} = 0, \quad \frac{\partial U}{\partial \varphi} \bigg|_{\varphi = \varphi_M} = 0 \quad (2)$$

and the resonance condition (1) was expanded by first derivative terms according to Ref. [36] to obtain better results for small values of  $\theta$  and  $\varphi$ . Here  $\omega$ ,  $\gamma$ ,  $M$ , and  $U$  denote the microwave's angular frequency, the gyromagnetic ratio, the magnetization, and the free-energy density, respectively. The free-energy density  $U$  consists of three contributions due to the Zeeman splitting  $U_{\text{Zee}} = -\mathbf{M} \cdot \mathbf{H}$ , the shape anisotropy  $U_{\text{shape}} = \mathbf{M} \cdot \hat{\mathbf{N}} \cdot \mathbf{M}$ , and the configurational anisotropy  $U_{\text{nu}} = K_{\text{nu}} \sin^2 \varphi \cos^2 \varphi$  (derived in analogy with cubic crystal anisotropy; see Ref. [37]) arising from the nonuniformity of the demagnetizing field [3,38]:

$$U = U_{\text{Zee}} + U_{\text{shape}} + U_{\text{nu}}. \quad (3)$$

$\mathbf{M}$ ,  $\mathbf{H}$ ,  $\hat{\mathbf{N}}$ , and  $K_{\text{nu}}$  denote the magnetization vector, the applied external magnetic field vector, the demagnetizing tensor, and a constant for describing the strength of the nonuniform demagnetization field, respectively. The angle dependence of two FMR resonances of sample Rect\_200 can be described by applying the Smit-Suhl formalism for two different values of the magnetization. The two values correspond to effective

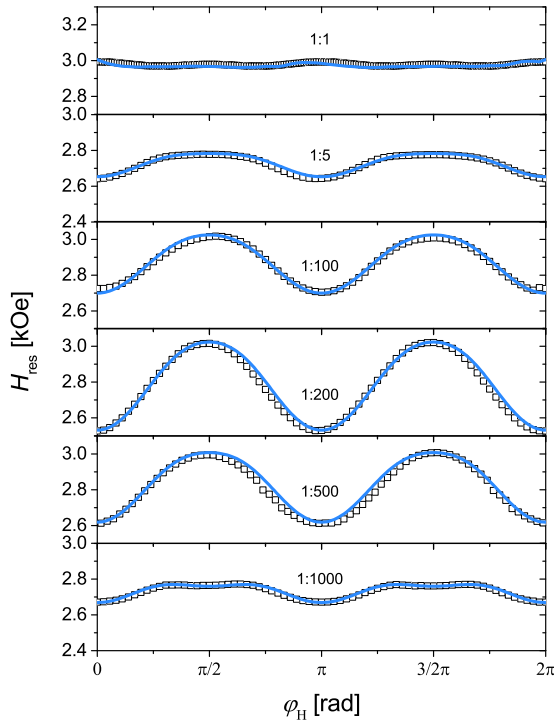


FIG. 5. Extracted values of the resonance field in in-plane geometry for various assemblies with different aspect ratios. The corresponding calculated curves derived with the Smit-Suhl formalism are also shown.

magnetizations reflecting the two maxima in the probability density function shown in Fig. 3(b). Good agreement between experiment and simulation is achieved for  $M_1 = 140 \text{ emu/cm}^3$  and  $M_2 = 70 \text{ emu/cm}^3$ , as shown in Fig. 4. However, it should be noted that, in particular, in the vicinity of  $\theta_H = 0$  the sharper signal corresponding to  $M_1 = 140 \text{ emu/cm}^3$  dominates the spectrum allowing us in the following to fit all in-plane spectra with only one FMR resonance of  $M_1 = 140 \text{ emu/cm}^3$ .

### B. Results for in-plane geometry

As pointed out above, it is justified to analyze the FMR measurements in in-plane geometry by fitting the spectra with only a single first derivative of a Lorentz resonance. The extracted resonance fields represent the dominant resonance of the two resonances arising in the nanoparticle assemblies. The typical in-plane angle dependence of the resonance field of samples with assemblies of different aspect ratios is shown in Fig. 5. The angle dependence of all assemblies except the one with an aspect ratio of 1:1 exhibits a pronounced twofold symmetry. Furthermore, for the two arrays of assemblies with an aspect ratio of 1:5 and 1:1000 the maxima at  $\varphi = \pi/2$  and  $\varphi = 3\pi/2$  exhibit slight indentations. Such behavior is expected for elongated nanomagnets. While the twofold symmetry arises from the elongated shape of the assemblies with an easy axis oriented along the assemblies' elongation direction, the indentations of the maxima can be attributed to nonuniform demagnetization fields, as discussed, for example, in Refs. [3,27,38].

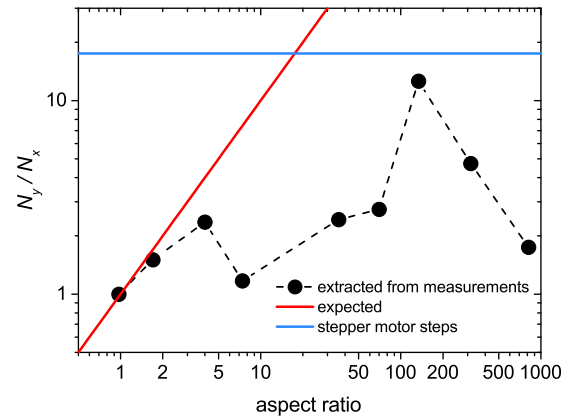


FIG. 6. Expected values for the ratio of  $N_y/N_x$  along with the extracted values from the calculation. The blue line above shows the maximum of the expected ratio due to the discrete stepper motor movement.

However, a closer look at the magnitude of the twofold symmetry reveals a more complicated behavior. While for aspect ratios below 1:200 the strength of the twofold symmetry increases as expected, it decreases again for the assemblies with the highest aspect ratios of 1:500 and 1:1000. In order to analyze this behavior in more detail, the Smit-Suhl formalism was used again to describe the angle dependence of the resonance field with respect to the orientation of the applied magnetic field. By simultaneous fitting of the resonance fields for the in-plane and out-of-plane geometries of each sample, it was possible to extract the demagnetization factors of the corresponding assemblies. The values of the demagnetization factors derived for all assemblies investigated are listed in Table I. Assuming a single-magnetic-domain structure in the assemblies, the ratio of the in-plane demagnetization factors  $N_y/N_x$  should be inversely proportional to the aspect ratio of the corresponding assembly, i.e.,  $N_y/N_x \propto x/y$ . As shown in Fig. 6, where the ratio of the demagnetization factors is plotted versus the aspect ratio of the assemblies determined from the analysis of SEM images, significant deviations from the expected behavior are observed. Although the determined ratio of the demagnetization factors (black circles) increases with increasing aspect ratio of the assemblies,  $N_y/N_x$  is much smaller than expected when assuming single-domain assemblies (red solid line). The ratio  $N_y/N_x$  significantly drops to a value of only 1.17 for the assembly Rect\_10 but increases again, reaching a maximum value of 12.68 for the assembly Rect\_200 with an aspect ratio of about 134. Finally, the ratio of the extracted demagnetization factors drops again to a value of only 1.76 for the assembly with the highest aspect ratio of about 815.

Keeping in mind that the theory of demagnetization used is applicable only for magnets consisting of a single domain [39], it may be concluded that the deviation between experiment and expectation is an indication of the formation of a multidomainlike structure inside the nanoparticle assemblies, as also observed in two-dimensional assemblies of cobalt nanoparticles [17,18].

### C. Micromagnetic simulations

Micromagnetic simulations were performed to explain the results obtained for the demagnetizing factors. Due to their organic surface coatings exchange coupling is not present between the single nanoparticles. They are distinct entities; that is, they share no common wave function. Thus, only dipolar interactions were taken into account for the micromagnetic simulations of the magnetic ordering in the assemblies. An atomistic model was used; that is, discrete spins were placed on a three-dimensional hexagonal grid with a lattice constant of 20 nm since such a hcp structure is the closest approximation to the experimental conditions. The spherical nanoparticles with a single magnetic moment were treated as a point dipole located in the origin of the sphere, as the interaction between two spheres is the same as between two dipoles as long as they do not overlap or are deformed otherwise [40]. For the magnetic moment  $m$  of each point dipole representing a nanoparticle, the magnetization of 140 kA/m found with FMR was multiplied by the volume  $V = 4\pi/3(d/2)^3$  of the nanoparticle, resulting in  $m = 63 \times 10^3 \mu_B$ , where  $\mu_B$  is the Bohr magneton. Nearest neighbors were considered up to the 32nd shell. Each shell contains all nearest neighbors at the same distance  $d_{NN}^i$ . Considering such a large number of shells is customary to properly account for the long-range dipole-dipole interaction. The system is evolved in time by the Landau-Lifshitz-Gilbert equation using the numerical parameters of  $\alpha = 0.1$  for the damping and  $\Delta t = 0.05$  as for the time steps. Calculations for different orientations of the magnetic field were performed to simulate the magnetic structure of the assemblies during the angle-dependent FMR measurements. The applied magnetic field is rather low as only dipolar interactions between the particles are considered and the magnetic moments will follow the applied field immediately. We calculated the magnetic structure of an assembly with an aspect ratio of 1:10 ( $x = 400$  nm,  $y = 4$   $\mu$ m) and five layers of nanoparticles in the  $z$  direction. We cut out two layers in the center to account for height differences in the assembly due to the nonhomogeneous filling observed in the openings as described above. This is shown schematically in Fig. 7(a). For a magnetic field orientation of  $\varphi_H = 0^\circ$  and  $\varphi_H = 45^\circ$  and a field strength of  $H = 500$  Oe the results are shown in Figs. 7(b) and 7(c), respectively. The calculations reveal that at the borders between the areas of different heights the magnetization shows inhomogeneities similar to the inhomogeneities at the edges of the assembly [see magnifications in Figs. 7(b) and 7(c)]. Therefore, the assembly is effectively divided into three magnetic domains with a drastically reduced aspect ratio compared to the assembly. Each domain behaves like a single magnet with respect to the applied magnetic field, resulting in a reduced ratio of the demagnetization factors as observed in the experiment. The origin of the height differences in the assemblies may be caused by the stepwise movement of the glass plate during the meniscus force deposition process. The stepper motor moves along the long axis of the assemblies with a step size of approximately 7.3  $\mu$ m every 30 s. During the time interval between these steps nanoparticles can assemble in areas of the PMMA opening where the meniscus is formed, while nanoparticles will assemble in the adjacent region if the stepper motor moves. From these considerations the maximum

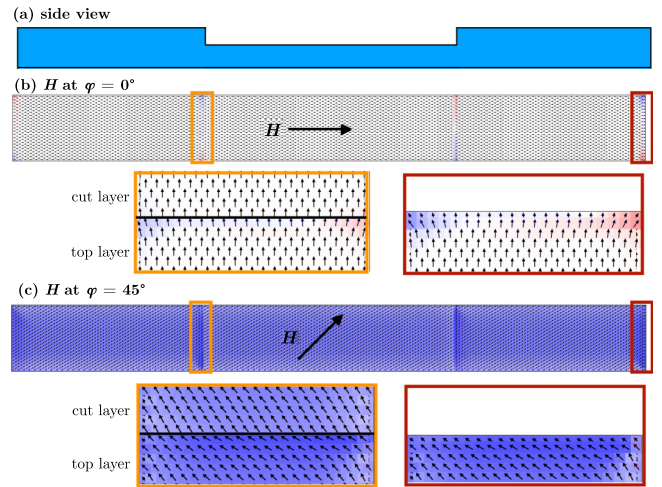


FIG. 7. (a) Schematic side view of the simulated assembly and results for the magnetization calculated for (b)  $H$  oriented parallel to the longer edge of the assembly, i.e.,  $\varphi_H = 0^\circ$ , and (c)  $\varphi_H = 45^\circ$  with  $H$  being at saturation. Scaled-up views of the border of the cut layers and the right edge of the assembly are marked; corresponding edges show the same behavior for the magnetization. OOMMF was used for visualization [41].

period of the height differences is given by the step size of the motor defining the maximum width of the corresponding domains in the assemblies. Taking a step size of 7.3  $\mu$ m and a width of the assemblies of 400 nm, a maximum value of the ratio of the demagnetization factors of 18.25 can be estimated. This value is shown in Fig. 6 as a blue line. It defines the upper limit for  $N_y/N_x$  in agreement with the experimental results. It should be noted that the height differences in the assemblies also impede the analysis of the angle-dependent FMR measurements using a diagonal demagnetizing tensor. In general, the elements of the diagonal demagnetizing tensor are calculated for rectangular magnetic prisms by averaging local demagnetizing factors  $N_{ij}(x, y, z)$  [42,43]. These local demagnetizing factors  $N_{ij}(x, y, z)$  are, however, calculated by discretizing an ideal rectangular prism into smaller prisms and considering the interactions between them [44,45]. Due to structural inhomogeneities, such as surface roughness or a porous structure, a magnetic structure exhibits additional magnetic inhomogeneities, which will not only modify the demagnetization factors  $N_{ij}(x, y, z)$  but also define new volumes where averaging is meaningful, e.g., regions of the same step height as in the case of our assemblies.

### IV. CONCLUSIONS

Magnetite nanoparticle assemblies with a rectangular shape and aspect ratios varying between 1:1 and 1:1000 were arranged using a horizontal dip-coating process on patterned substrates prepared using electron-beam lithography. The magnetic properties of the assemblies were investigated using angle-dependent ferromagnetic resonance measurements. In the out-of-plane geometry two resonances are observed which arise due to the random orientation of the nanoparticles in the assemblies. For a magnetic field orientation in the sample plane both resonances overlap, resulting in one broad resonance

line. The angle dependence of the resonance fields for both geometries were described using the Smit-Suhl formalism yielding the demagnetization factors of the corresponding structure. For assemblies with small aspect ratios, the inverse ratio of the in-plane demagnetization tensors is in good agreement with the aspect ratio of the corresponding assemblies, while for larger structures the determined values differ from the aspect ratio of the rectangular assemblies. This result is attributed to a multidomain structure caused by structural inhomogeneities in the nanoparticle assemblies, leading to smaller volumes where averaging of the demagnetizing factors is meaningful. The formation of such a domain structure due to structural inhomogeneities is qualitatively supported by micromagnetic simulations. Thus, care must be taken when

demagnetization is taken into account in the description of such assemblies consisting of nanomagnets. It is important to note that the pitch of the structural inhomogeneities can be controlled in the fabrication process of the assemblies. This control offers additional degrees of freedom for tuning the magnetic interactions for future applications.

### ACKNOWLEDGMENTS

The authors would like to thank Dr. H.-A. Krug von Nidda and D. Ehlers of the Institut für Physik of the Universität Augsburg for providing the program used for fitting the experimental spectra. Simulations were performed on the high-performance cluster of the ZfM/LaMa.

- 
- [1] Y. Köseoğlu, H. Kavas, and B. Aktaş, *Phys. Status Solidi A* **203**, 1595 (2006).
- [2] B. D. Terris and T. Thomson, *J. Phys. D* **38**, R199 (2005).
- [3] R. Cowburn, *J. Magn. Magn. Mater.* **242**, 505 (2002).
- [4] R. P. Cowburn and M. E. Welland, *Science* **287**, 1466 (2000).
- [5] C. A. Ross, *Annu. Rev. Mater. Res.* **31**, 203 (2001).
- [6] P. Li, G. Csaba, V. K. Sankar, X. Ju, P. Lugli, X. S. Hu, M. Niemier, W. Porod, and G. H. Bernstein, *J. Appl. Phys.* **111**, 07B911 (2012).
- [7] A. Imre, G. Csaba, L. Ji, A. Orlov, G. H. Bernstein, and W. Porod, *Science* **311**, 205 (2006).
- [8] Y. Zhang, L. Sun, Y. Fu, Z. C. Huang, X. J. Bai, Y. Zhai, J. Du, and H. R. Zhai, *J. Phys. Chem. C* **113**, 8152 (2009).
- [9] K. Yakushiji, F. Ernult, H. Imamura, K. Yamane, S. Mitani, K. Takanashi, S. Takahashi, S. Maekawa, and H. Fujimori, *Nat. Mater.* **4**, 57 (2005).
- [10] P. Landeros, J. Escrig, D. Altbir, D. Laroze, J. d'Albuquerque e Castro, and P. Vargas, *Phys. Rev. B* **71**, 094435 (2005).
- [11] R. P. Cowburn, *Phys. Rev. B* **65**, 092409 (2002).
- [12] R. P. Cowburn, *J. Phys. D* **33**, R1 (2000).
- [13] M. Schneider and H. Hoffmann, *J. Appl. Phys.* **86**, 4539 (1999).
- [14] M. Hanson, R. Bručas, T. J. Antosiewicz, R. K. Dumas, B. Hjörvarsson, V. Flovik, and E. Wahlström, *Phys. Rev. B* **92**, 094436 (2015).
- [15] R. D. Gomez, T. V. Luu, A. O. Pak, K. J. Kirk, and J. N. Chapman, *J. Appl. Phys.* **85**, 6163 (1999).
- [16] A. Lebib, S. P. Li, M. Natali, and Y. Chen, *J. Appl. Phys.* **89**, 3892 (2001).
- [17] M. Varón, M. Beleggia, T. Kasama, R. J. Harrison, R. E. Dunin-Borkowski, V. F. Puentes, and C. Frandsen, *Sci. Rep.* **3**, 1234 (2013).
- [18] M. Varón, M. Beleggia, J. Jordanovic, J. Schioz, T. Kasama, V. F. Puentes, and C. Frandsen, *Sci. Rep.* **5**, 14536 (2015).
- [19] D. Toulemon, M. V. Rastei, D. Schmool, J. S. Garitaonandia, L. Lezama, X. Cattoën, S. Bégin-Colin, and B. P. Pichon, *Adv. Funct. Mater.* **26**, 2454 (2016).
- [20] V. F. Puentes, P. Gorostiza, D. M. Aruguete, N. G. Bastus, and A. P. Alivisatos, *Nat. Mater.* **3**, 263 (2004).
- [21] M. Kure, M. Beleggia, and C. Frandsen, *J. Appl. Phys.* **122**, 133902 (2017).
- [22] S. L. Tripp, R. E. Dunin-Borkowski, and A. Wei, *Angew. Chem., Int. Ed.* **42**, 5591 (2003).
- [23] S. Sun, C. B. Murray, D. Weller, L. Folks, and A. Moser, *Science* **287**, 1989 (2000).
- [24] S. B. Clendenning, S. Fournier-Bidoz, A. Pietrangelo, G. Yang, S. Han, P. M. Brodersen, C. M. Yip, Z.-H. Lu, G. A. Ozin, and I. Manners, *J. Mater. Chem.* **14**, 1686 (2004).
- [25] S. Singamaneni, V. N. Bliznyuk, C. Binek, and E. Y. Tsymlal, *J. Mater. Chem.* **21**, 16819 (2011).
- [26] Z. Nie, A. Petukhova, and E. Kumacheva, *Nat. Nanotechnol.* **5**, 15 (2010).
- [27] A. Fabian, M. T. Elm, D. M. Hofmann, and P. J. Klar, *J. Appl. Phys.* **121**, 224303 (2017).
- [28] S. Ni, J. Leemann, H. Wolf, and L. Isa, *Faraday Discuss.* **181**, 225 (2015).
- [29] S. Mehraeen, M. Asbahi, W. Fuke, J. K. W. Yang, J. Cao, and M. C. Tan, *Langmuir* **31**, 8548 (2015).
- [30] I. S. Poperechny and Y. L. Raikher, *Phys. Rev. B* **93**, 014441 (2016).
- [31] M. Winklhofer, L. Chang, and S. H. K. Eder, *Geochem. Geophys. Geosyst.* **15**, 1558 (2014).
- [32] M. Charilaou, M. Winklhofer, and A. U. Gehring, *J. Appl. Phys.* **109**, 093903 (2011).
- [33] V. A. Ivanshin, J. Deisenhofer, H.-A. Krug von Nidda, A. Loidl, A. A. Mukhin, A. M. Balbashov, and M. V. Eremin, *Phys. Rev. B* **61**, 6213 (2000).
- [34] J. Smit and H. G. Beljers, *Philips Res. Rep.* **10**, 113 (1955).
- [35] H. Suhl, *Phys. Rev.* **97**, 555 (1955).
- [36] *Magnetic Nanoparticles*, edited by S. P. Gubin (Wiley-VCH, Weinheim, Germany, 2009).
- [37] J. García-Otero, M. Porto, J. Rivas, and A. Bunde, *J. Appl. Phys.* **85**, 2287 (1999).
- [38] R. P. Cowburn, A. O. Adeyeye, and M. E. Welland, *Phys. Rev. Lett.* **81**, 5414 (1998).
- [39] J. A. Osborn, *Phys. Rev.* **67**, 351 (1945).
- [40] B. F. Edwards, D. M. Riffe, J.-Y. Ji, and W. A. Booth, *Am. J. Phys.* **85**, 130 (2017).
- [41] The OOMMF code is available at <http://math.nist.gov/oommf>.
- [42] A. Aharoni, *J. Appl. Phys.* **83**, 3432 (1998).
- [43] M. Schabes and A. Aharoni, *IEEE Trans. Magn.* **23**, 3882 (1987).
- [44] A. J. Newell, W. Williams, and D. J. Dunlop, *J. Geophys. Res.* **98**, 9551 (1993).
- [45] A. Bagnérés-Viallix and P. Baras, *Br. J. Appl. Phys.* **69**, 4599 (1991).